Research Square

Preprints are preliminary reports that have not undergone peer review.
They should not be considered conclusive, used to inform clinical practice,
or referenced by the media as validated information.

Robust Bilayer Electronic Structure and Reduced Magnetic Exchange in La2SmNi2O7

Xinru Huang
Beijing Normal University, Beijing Normal University, Ministry of Education
Jiaxin Yan
Shandong University
Ruixian Liu
Beijing Normal University, Beijing Normal University, Ministry of Education
Zhijia Zhang
Swiss Light Source, Paul Scherrer Institut
Anni Chen
Swiss Light Source, Paul Scherrer Institut
Yating Luo
Beijing Normal University, Beijing Normal University, Ministry of Education
Hengyang Zhong
Beijing Normal University, Beijing Normal University, Ministry of Education
Xinman Ye
Sun Yat-Sen University
Daniel Foster
Japan Synchrotron Radiation Research Institute (JASRI)
Hiroki Suga
Japan Synchrotron Radiation Research Institute (JASRI)
Jun Miyawaki
National Institutes for Quantum Science and Technology
Dao-Xin Yao
Sun Yat-Sen University
Junjie Zhang
Shandong University
Thorsten Schmitt
Swiss Light Source, Paul Scherrer Institut
Xingye Lu
luxy@bnu.edu.cn

Beijing Normal University, Beijing Normal University, Ministry of Education

Article

Keywords:

Posted Date: October 16th, 2026

DOI: https://doi.org/10.21203/rs.3.rs-11182632/v1

License: This work is licensed under a Creative Commons Attribution 4.0 International License.
Read Full License

Additional Declarations: No competing interests reported.

Robust Bilayer Electronic Structure and Reduced Magnetic Exchange in $La_2SmNi_2O_7$

Xinru Huang,[1,*] Jiaxin Yan,[2,*] Ruixian Liu,[1] Zhijia Zhang,[3] Anni Chen,[3] Yating Luo,[1] Hengyang Zhong,[1] Xinman Ye,[4] Daniel Foster,[5] Hiroki Suga,[5] Jun Miyawaki,[6] Dao-Xin Yao,[4] Junjie Zhang,[2,†] Thorsten Schmitt,[3,‡] and Xingye Lu[1,§]

[1]*School of Physics and Astronomy, Beijing Normal University, and Key Laboratory of Multiscale Spin Physics (Beijing Normal University), Ministry of Education, Beijing 100875, China*
[2]*State Key Laboratory of Crystal Materials, Institute of Crystal Materials, Shandong University, Jinan 250100, China*
[3]*Photon Science Division, Swiss Light Source, Paul Scherrer Institut, CH-5232 Villigen PSI, Switzerland*
[4]*Guangdong Provincial Key Laboratory of Magnetoelectric Physics and Devices, School of Physics, Sun Yat-Sen University, Guangzhou 510275, China*
[5]*Japan Synchrotron Radiation Research Institute (JASRI) 468-1, Aramaki Aza Aoba, Sendai, Miyagi, 980-8572, Japan*
[6]*NanoTerasu Center, National Institutes for Quantum Science and Technology, 468-1, Aoba, Aramaki, Aoba-ku, Sendai, Miyagi, 980-8572, Japan*

(Dated: September 27, 2026)

Rare-earth substitution provides an effective route to enhance superconductivity in bilayer nickelates, but its influence on the local electronic structure and magnetic exchange interactions remains unclear. Here we report Ni-L_3-edge resonant inelastic x-ray scattering (RIXS) measurements on single crystals of $La_2SmNi_2O_7$, a Sm-substituted bilayer nickelate with enhanced in-plane lattice distortion and a reduced interlayer Ni–O_{AP}–Ni bond angle. Despite these structural modifications, the local electronic excitations associated with NiO_6 crystal-field and charge-transfer processes occur at essentially the same energies as in $La_3Ni_2O_7$, including features near 0.3 eV, 1.0 eV, and 1.5 eV. This shows that Sm substitution does not substantially alter the local NiO_6 crystal-field and charge-transfer energy scales of the corner-shared bilayer. In contrast, high-resolution RIXS reveals well-defined spin-wave-like excitations whose band top is reduced by ~ 7 meV. A bilayer J_c-J_1-J_2 Heisenberg analysis of the spin excitation dispersion indicates an approximately 10% reduction of the effective magnetic exchange scale, which correlates with the reduced interlayer Ni–O_{AP}–Ni bond angle. The small intrinsic damping of these modes further points to robust local-moment-like spin dynamics in the ambient-pressure parent phase. These results reveal a dichotomy in the response to Sm substitution, with largely preserved local electronic excitation energies but a reduced magnetic exchange scale. They identify the Ni–O_{AP}–Ni geometry as an important structural parameter influencing magnetism in Ruddlesden–Popper nickelates and provide spectroscopic constraints on microscopic models of high-T_c superconductivity in this family.

The bilayer Ruddlesden–Popper nickelates have recently emerged as a new platform for high-temperature superconductivity. In the prototypical compound $La_3Ni_2O_7$, superconductivity with $T_{c,\mathrm{onset}}$ near 80 K appears under hydrostatic pressure, placing this material family among the few non-cuprate systems with transition temperatures approaching the liquid-nitrogen scale [1–5]. Subsequent work has shown that isovalent rare-earth substitution on the La site can stabilize and further enhance the bulk superconducting phase, with $La_{3-x}R_xNi_2O_7$ (R = Pr, Sm, Nd) reaching $T_{c,\mathrm{onset}}$ up to $\sim$ 100 K under pressure [6–10]. More recently, compressive epitaxial strain on $SrLaAlO_4$(001) substrate has enabled ambient-pressure superconductivity in $La_3Ni_2O_7$-based films, with reported onset temperatures above 40 K and approaching 60 K in recent studies [11–15]. Together, these results establish pressure, epitaxial strain, and rare-earth substitution as effective tuning parameters for superconductivity in bilayer nickelates.

$La_3Ni_2O_7$ is built from corner-shared NiO_6 bilayers, in which adjacent NiO_2 planes are coupled through inner apical oxygens (O_{AP}). This geometry generates a prominent interlayer d_{z^2}–O_{AP}–d_{z^2} pathway, while both Ni $3d_{x^2-y^2}$ and $3d_{z^2}$ orbitals contribute to the Fermi surface and low-energy electronic structure [1, 16–28]. Ni-L_3-edge RIXS measurements further resolved local electronic excitations involving Ni $3d$ orbitals and ligand-hole states, together with a spin-density-wave (SDW) transition near 150 K and dispersive spin excitations governed by sizable interlayer superexchange interactions [16]. These observations have motivated theoretical proposals in which interlayer antiferromagnetic exchange and spin fluctuations play central roles in superconductivity [27, 29–31]. Recent neutron and resonant x-ray studies have established stripe-type SDW correlations in $La_3Ni_2O_7$ [32–36]. Experiments on pressure- and oxygen-tuned $La_3Ni_2O_7$ further show that tetragonal symmetry or a straightened Ni–O–Ni bond alone is insufficient to ensure superconductivity, pointing instead to an interplay of local structure and density-wave correlations [4].

Among rare-earth-substituted bilayer nickelates, $La_2SmNi_2O_7$ has emerged as a particularly important high-T_c member, exhibiting bulk superconductivity under hydrostatic pressure with $T_{c,\max}^{\mathrm{onset}} = 92$ K and $T_{c,\max}^{\mathrm{zero}} = 73$ K at 21.6 GPa [7]. It retains the bilayer Ruddlesden–Popper framework but crystallizes in a monoclinic structure. Relative to $La_3Ni_2O_7$, the ambient-pressure in-plane lattice distortion $\Delta = (a-b)/(a+b)$ increases from $\sim 3.6 \times 10^{-3}$ to $\sim 8.6 \times 10^{-3}$, while reported values of the interlayer Ni–O_{AP}–Ni bond angle decrease from approximately 168° to the 162°–164° range [1, 4, 7, 37]. Similar to $La_3Ni_2O_7$, magnetic susceptibility measurements on $La_2SmNi_2O_7$ reveal a signature consistent with static SDW order [7]. Transport measurements further indicate that the normal-state conduc-

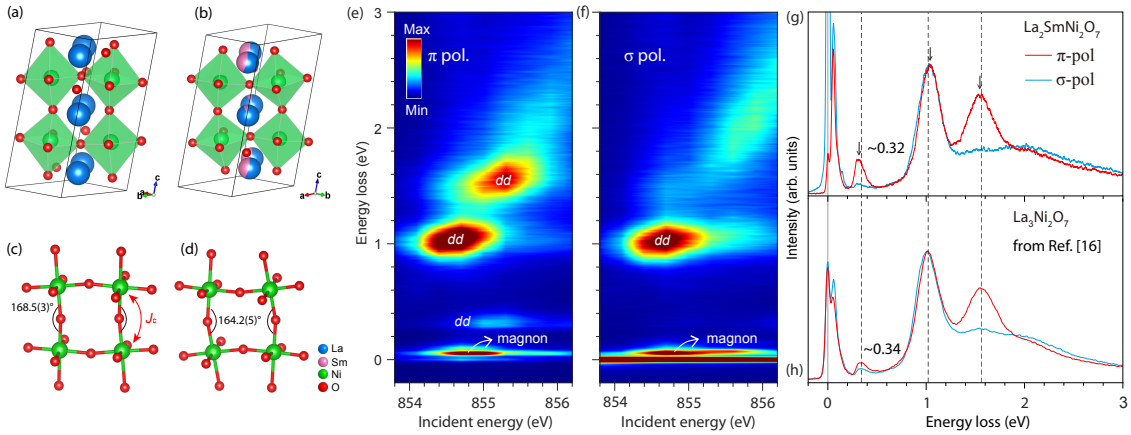


FIG. 1. Local structure and Ni-L_3 RIXS spectra of $La_2SmNi_2O_7$. (a),(b) Crystal structures of monoclinic $La_3Ni_2O_7$ and $La_2SmNi_2O_7$ ($P2_1/m$), respectively. (c),(d) Ball-and-stick representations of the corner-shared NiO_6 bilayers, with the interlayer Ni–O_{AP}–Ni bond angles reported in Ref. [7] indicated. (e),(f) Incident-energy-dependent Ni-L_3-edge RIXS intensity maps of $La_2SmNi_2O_7$ measured with π- and σ-polarized incident light, respectively. The measurements were performed at $T = 20$ K with a scattering angle $2\theta = 90°$ and an incident angle $\theta = 20°$. (g) Corresponding incident-energy-integrated spectra of $La_2SmNi_2O_7$ obtained from (e),(f) over the incident-energy range 853.8–856.2 eV. (h) Incident-energy-integrated Ni-L_3 RIXS spectra of $La_3Ni_2O_7$, reproduced from Ref. [16]. Black dashed lines mark the peak energies of the electronic excitations in $La_3Ni_2O_7$, while black arrows indicate the corresponding peak positions in $La_2SmNi_2O_7$. The spectra show closely comparable local electronic excitations in the two compounds, with the lowest-energy feature shifting only modestly from ~ 0.34 eV in $La_3Ni_2O_7$ to ~ 0.32 eV in $La_2SmNi_2O_7$.

tivity of Sm-substituted bilayer nickelates depends on sample form and pressure: polycrystalline $La_{2.1}Sm_{0.9}Ni_2O_7$ samples show semiconducting behavior at ambient pressure [8], whereas single-crystal $La_2SmNi_2O_7$ develops metallic-like transport under approximately 3 GPa [7]. Complementary powder inelastic neutron scattering (INS) measurements on Pr- and Nd-substituted bilayer nickelates found that the spin-fluctuation modes and effective interlayer couplings vary with the substituted rare-earth ion, indicating that the magnetic energy scale does not follow a single systematic trend across different rare-earth substitutions [38].

This combination of enhanced pressure-induced superconductivity, stronger local structural distortion, and a reported SDW-related signature raises fundamental questions about how local structural degrees of freedom govern the electronic and magnetic properties of bilayer nickelates. In particular, the strong involvement of the Ni $3d_{z^2}$ orbital and the interlayer Ni–O_{AP}–Ni pathway suggests that subtle structural modifications may strongly influence the low-energy electronic states and magnetic exchange interactions. It also remains unclear how the underlying dynamic spin correlations evolve when static SDW signatures are weak. $La_2SmNi_2O_7$ therefore offers a timely opportunity to examine how rare-earth-induced modifications of the NiO_6 bilayer influence the local electronic structure and magnetic exchange interactions, thereby providing insight into the microscopic ingredients relevant to high-T_c superconductivity in bilayer nickelates.

In this work, we use Ni-L_3-edge RIXS to determine how the Sm-induced distortion of the NiO_6 bilayer modifies the local electronic excitations and spin dynamics, by directly comparing $La_2SmNi_2O_7$ with $La_3Ni_2O_7$ [1, 7, 16]. Despite the enhanced in-plane lattice distortion and reduced interlayer Ni–O_{AP}–Ni bond angle in $La_2SmNi_2O_7$, the characteristic dd excitation energies remain nearly unchanged from those of $La_3Ni_2O_7$. This shows that Sm substitution does not substantially alter the local NiO_6 crystal-field and charge-transfer excitation energies, including modes involving out-of-plane Ni d_{z^2}–O_{AP} p_z hybridization. In the low-energy channel, we resolve clear, weakly damped dispersive magnetic excitations in $La_2SmNi_2O_7$, whose band top is reduced by about 7 meV compared with $La_3Ni_2O_7$. A fit to a bilayer J_c-J_1-J_2 Heisenberg model shows that the effective exchange scale is reduced by approximately 10%, a change that correlates with the reduction of the reported interlayer Ni–O_{AP}–Ni bond angle from $\sim 168°$ in $La_3Ni_2O_7$ to $164.2°$ in $La_2SmNi_2O_7$. Taken together, these results reveal a dichotomy in the response of the excitation spectrum to Sm substitution. The local NiO_6 crystal-field and charge-transfer excitation energies remain largely preserved, whereas the spin-excitation band top and the effective magnetic exchange scale are reduced. The persistence of well-defined magnetic excitations supports a local-moment-like description of the spin dynamics, while their reduced energy scale points to the Ni–O_{AP}–Ni bond geometry as an important structural parameter influencing magnetism in Ruddlesden–Popper nickelates.

The $La_2SmNi_2O_7$ single crystals used in this work were grown at ambient pressure by a K_2CO_3-flux evaporation method and postannealed under oxygen pressure, $p_{O_2} = 1.5$ bar, for 10 days to reduce oxygen deficiency, following Ref. [7]. The annealed crystals are essentially stoichiometric within the uncertainty of thermogravimetric analysis. Ni-L_3-edge RIXS measurements were performed at the BL02U

beamline of the NanoTerasu synchrotron light source with a nominal combined energy resolution of $\Delta E \approx 22$ meV. All spectra were collected at $T = 20$ K.

Figures 1(a)–1(d) compare the local bilayer structures of $La_3Ni_2O_7$ and $La_2SmNi_2O_7$. Both compounds consist of corner-shared NiO_6 bilayers, but Sm substitution substantially modifies the local geometry. Previous scanning transmission electron microscopy (STEM) and single-crystal X-ray diffraction (SXRD) studies showed that Sm preferentially occupies the La site between adjacent bilayers, thereby stabilizing an ordered bilayer stacking in $La_2SmNi_2O_7$ [7]. Compared with $La_3Ni_2O_7$, the crystallographic c axis of $La_2SmNi_2O_7$ is shortened by about 1.2% [4, 7]. However, the geometric Ni–Ni distance across the inner apical oxygen within a bilayer, estimated from the reported Ni–O bond lengths and Ni–O_{AP}–Ni bond angle, shows no appreciable change between the two compounds and stays close to $\sim$ 3.94 Å [4, 7]. The dominant local structural change is instead the reduction of the interlayer Ni–O_{AP}–Ni bond angle from $\sim$ 168° to 164.2°, together with an enhanced in-plane lattice distortion, which lowers the local symmetry of the NiO_6 octahedra. A recent synchrotron single-crystal x-ray diffraction study verified the monoclinic structure at ambient pressure but reported a different space group and an even smaller Ni–O_{AP}–Ni bond angle of 162°, further corroborating the reduction of the interlayer bond angle in $La_2SmNi_2O_7$ [37].

To assess the sensitivity of the local electronic excitation spectrum to these Sm-induced structural modifications, we first performed incident-energy-dependent Ni-L_3-edge RIXS measurements on $La_2SmNi_2O_7$ and compared the resulting electronic excitations with those reported for $La_3Ni_2O_7$ [16]. Figures 1(e) and 1(f) show the incident-energy-dependent Ni-L_3-edge RIXS intensity maps of $La_2SmNi_2O_7$ measured with π- and σ-polarized incident light, respectively. The corresponding incident-energy-integrated spectra are compared with those of $La_3Ni_2O_7$ in Figs. 1(g) and 1(h). Despite the enhanced local distortion and the reduced interlayer Ni–O_{AP}–Ni bond angle in $La_2SmNi_2O_7$, the two compounds exhibit closely similar excitation spectra. In both cases, we observe a low-energy magnetic excitation below 0.1 eV, together with characteristic electronic excitations near 0.3–0.4 eV, 1.0 eV, and 1.5–1.6 eV.

These features also show similar polarization dependence in the two compounds. In particular, the 0.3–0.4 eV and 1.5–1.6 eV modes are both enhanced for π polarization and appear in a similar incident-energy range, suggesting a common sensitivity to out-of-plane Ni–O electronic states. The $\sim$ 1.0 eV excitation can be assigned to a local dd transition between the t_{2g} and e_g sectors, as commonly observed in octahedral nickelates [16, 20]. Previous analyses of $La_3Ni_2O_7$ attributed the 0.3–0.4 eV and 1.5–1.6 eV features to mixed dd and charge-transfer excitations involving Ni $3d$ orbitals and ligand-hole states, consistent with their stronger π-polarized intensity and their sensitivity to the out-of-plane Ni d_{z^2}–O_{AP} p_z sector [16, 39]. The clearest difference between the two compounds is a modest softening of the 0.3–0.4 eV mode,

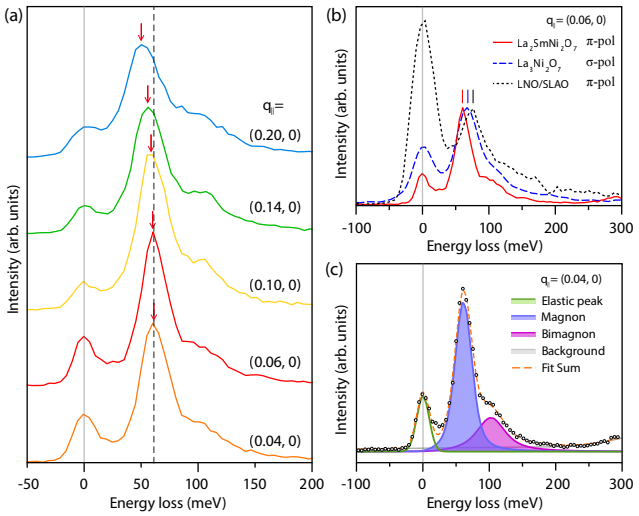


FIG. 2. Well-defined dispersive spin excitations in $La_2SmNi_2O_7$. (a) Waterfall plot of Ni-L_3-edge RIXS spectra measured along the $[H, 0]$ direction using π-polarized incident photons with $E_i = 854.65$ eV at $T = 20$ K. Well-defined dispersive magnetic excitations are observed. Red arrows mark the peak positions of the spin excitations. (b) Comparison of spin-excitation spectra at $q_\parallel = (0.06, 0)$, close to the band top near the zone center, for $La_2SmNi_2O_7$, bulk $La_3Ni_2O_7$, and $La_3Ni_2O_7$/$SrLaAlO_4$. Short vertical ticks indicate the fitted magnon peak positions. The data for $La_3Ni_2O_7$ and $La_3Ni_2O_7$/$SrLaAlO_4$ are reproduced from Refs. [16, 40]. (c) Representative resolution-convolved DHO fit to the RIXS spectrum of $La_2SmNi_2O_7$ at $q_\parallel = (0.04, 0)$. For this spectrum, the experimental resolution function was determined from the fitted elastic line, giving an energy-resolution FWHM of $\Delta E \approx 20$ meV. The shaded components denote elastic scattering, one-magnon and bimagnon excitations, together with an empirical high-energy background. The dashed curve represents the total fit.

from $\sim$ 0.34 eV in $La_3Ni_2O_7$ to approximately $\sim$ 0.32 eV in $La_2SmNi_2O_7$. Overall, these results show that Sm substitution does not substantially alter the local NiO_6 crystal-field and charge-transfer excitation energies of the corner-shared bilayer.

The low-energy region of the spectra in Figs. 1(g) and 1(h) already reveals a pronounced magnetic excitation below 0.1 eV in $La_2SmNi_2O_7$, suggesting that the reported SDW-related signature is accompanied by strong dynamic spin correlations. To directly probe the underlying spin dynamics, we performed high-resolution Ni-L_3-edge RIXS measurements near the Γ point, where the stripe-order-derived spin-wave dispersion of $La_3Ni_2O_7$ reaches its band maximum and is particularly sensitive to the interlayer exchange interaction [16]. Figure 2(a) presents a waterfall plot of the RIXS spectra measured along the H direction for $q_\parallel = (0.04, 0)$–$(0.20, 0)$. Well-defined magnetic peaks are clearly resolved throughout this momentum range. The dashed vertical line marks the peak position at $q_\parallel = (0.04, 0)$, while arrows indicate the corresponding peak positions at all momenta. The systematic momentum-dependent energy shift demonstrates that these excitations are dispersive spin-wave-like modes

rather than localized crystal-field excitations. The spectrum at $q_{\parallel} = (0.06, 0)$, close to the band top near Γ, enables a direct comparison among $La_2SmNi_2O_7$, bulk $La_3Ni_2O_7$, and $La_3Ni_2O_7$/$SrLaAlO_4$ (LNO/SLAO) [Fig. 2(b)] [40]. The excitation energy increases across this series as the reported interlayer Ni–O_{AP}–Ni bond angle becomes straighter, evolving from 164.2° in $La_2SmNi_2O_7$ to approximately $\sim 168°$ in bulk $La_3Ni_2O_7$ and approaching 180° in LNO/SLAO [7, 40, 41]. This correlation indicates that the spin-excitation energy scale is sensitive to the interlayer bond geometry and is consistent with an important contribution from the Ni d_{z^2}–O_{AP} p_z–Ni d_{z^2} superexchange pathway.

To quantitatively determine the excitation energies and damping parameters, the low-energy spectra were analyzed using a resolution-convolved damped harmonic oscillator (DHO) model to account for instrumental broadening. The intrinsic response is $\chi''(q, E) \propto \gamma_q E/[(E^2 - E_{0,q}^2)^2 + 4\gamma_q^2 E^2]$, where E is the energy loss, $E_{0,q}$ is the undamped mode energy, and γ_q is the intrinsic damping parameter. For $La_2SmNi_2O_7$, the momentum-dependent resolution function was determined independently for each spectrum from the elastic-line fit and fixed in the DHO analysis. A representative fit at $q_{\parallel} = (0.04, 0)$ is shown in Fig. 2(c). The spectrum is well described by a sharp, weakly damped magnon mode together with a higher-energy bimagnon excitation, demonstrating that well-defined magnetic excitations are present in the low-temperature state where an SDW-related signature has been reported. For comparison, the published $La_3Ni_2O_7$ spectra [16] were reanalyzed using the reported instrumental resolution. Further details of the spectral models, fitting uncertainties, and the relation between the intrinsic mode energies and spectral peak positions are provided in the Supplemental Material. The resulting undamped mode energies $E_{0,q}$ of $La_2SmNi_2O_7$ are summarized in Fig. 3 (red circles). Throughout the measured momentum range, the excitations lie systematically below those of $La_3Ni_2O_7$, indicating a modest reduction of the spin-excitation band top and magnetic energy scale.

The reported SDW-related signature in $La_2SmNi_2O_7$, together with several spectroscopic observations, motivates using the stripe-order-derived spin-wave framework established for $La_3Ni_2O_7$ as an effective description [16, 32]. The magnetic excitations are sharp and dispersive near the band maximum, and their momentum dependence closely follows that of $La_3Ni_2O_7$. We therefore use the stripe-based bilayer Heisenberg model as a minimal parameterization of the stripe-like spin correlations in $La_3Ni_2O_7$ and $La_2SmNi_2O_7$, rather than as an independent determination of the exact static spin structure in $La_2SmNi_2O_7$.

To model the dispersion, we adopted a reduced bilayer Heisenberg Hamiltonian based on the stripe spin-wave framework established by inelastic neutron scattering on $La_3Ni_2O_7$ [32],

$$\mathcal{H} = J_c \sum_i \mathbf{S}_{i,t}\cdot\mathbf{S}_{i,b} + J_1 \sum_{\langle i,j\rangle,\alpha} \mathbf{S}_{i,\alpha}\cdot\mathbf{S}_{j,\alpha} + J_2 \sum_{\langle\langle i,j\rangle\rangle,\alpha} \mathbf{S}_{i,\alpha}\cdot\mathbf{S}_{j,\alpha},$$

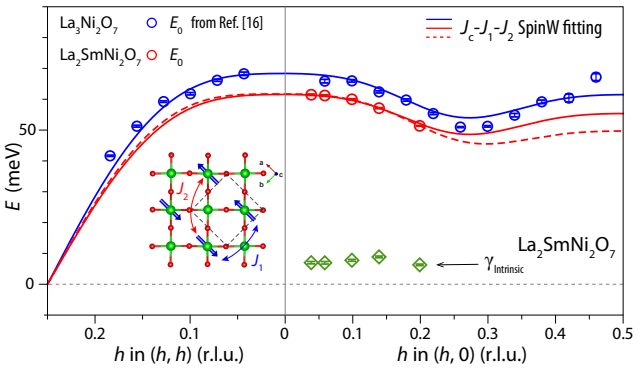


FIG. 3. Dispersion and intrinsic damping of spin excitations in $La_2SmNi_2O_7$. Red open circles show the undamped mode energies $E_{0,q}$ of $La_2SmNi_2O_7$ extracted from resolution-convolved DHO fits to the RIXS spectra, with a representative fit shown in Fig. 2(c). Green open diamonds show the intrinsic damping parameters γ_q obtained from the same convolved fits. For each $La_2SmNi_2O_7$ spectrum, the resolution function was determined from a Pearson-VII fit to the elastic line. For comparison, blue open circles show the corresponding $E_{0,q}$ values of $La_3Ni_2O_7$, obtained by reanalyzing the source spectra of Ref. [16] with a 36.5-meV-FWHM Gaussian resolution function. The blue solid curve is a bilayer J_c-J_1-J_2 SpinW fit to the $La_3Ni_2O_7$ dispersion. The red solid and dashed curves show, respectively, the common-scale fit with $s = 0.90$ and the free-parameter fit to the five $La_2SmNi_2O_7$ data points. The inset illustrates the assumed single-stripe spin configuration and defines the exchange-parameter convention. The vertical gray line marks the Γ point. Error bars denote formal standard errors from the spectral fits.

where $\alpha = t, b$ denotes the top and bottom NiO_2 layers within a bilayer. The interlayer exchange J_c couples Ni spins across the inner apical oxygen [Fig. 1(c)], whereas J_1 and J_2 denote the in-plane nearest-neighbor and next-nearest-neighbor exchange couplings, respectively, following the convention illustrated in the inset of Fig. 3. Compared with the full neutron spin-wave model, which distinguishes the anisotropic nearest-neighbor terms J_{1a} and J_{1b} and includes a small anisotropy term, the present reduced model uses an effective J_1 and focuses on the exchange energy scale constrained by the RIXS data near the band maximum.

An unweighted least-squares fit of the reanalyzed $La_3Ni_2O_7$ dispersion to the linear spin-wave branch of this model gives $SJ_c = 36.4 \pm 4.8$ meV, $SJ_1 = 1.53 \pm 0.37$ meV, and $SJ_2 = 7.27 \pm 0.68$ meV. The fitted band top near Γ is 68.4 ± 1.8 meV [blue solid curve in Fig. 3]. The fitted interlayer exchange scale is consistent within uncertainty with the neutron-scattering value of $SJ_c = 39.86 \pm 0.85$ meV [32], supporting a substantial interlayer exchange contribution. Because the $La_2SmNi_2O_7$ data cover only five momenta near the band maximum, we avoid overparameterizing the fit. Instead, we use the $La_3Ni_2O_7$ exchange parameters as a reference and scale them by a common factor to reproduce the $La_2SmNi_2O_7$ dispersion. This common-scale parameterization provides a minimal comparison of the magnetic energy scales without assuming that each microscopic coupling is independently de-

termined. Such an overall reduction is also qualitatively consistent with the structural changes in $La_2SmNi_2O_7$, where the interlayer Ni–O_{AP}–Ni bond angle decreases from approximately 168° to 164.2° and the in-plane Ni–O–Ni bonds are more strongly bent away from 180°, both of which can modify oxygen-mediated hopping and superexchange pathways [42–45]. The best scaled fit yields a factor of 0.90, corresponding to an approximately 10% reduction of the effective exchange scale in $La_2SmNi_2O_7$. The resulting band top is 61.5 meV [red solid curve in Fig. 3], about 6.9 meV below the $La_3Ni_2O_7$ reference.

As a consistency check, we also fitted the five $La_2SmNi_2O_7$ energies with three independent exchange parameters. This free-parameter fit gives $SJ_c = 31.0$ meV, $SJ_1 = 2.7$ meV, and $SJ_2 = 6.33$ meV, with a band top of 61.7 meV [red dashed curve in Fig. 3]. Both the common-scale and free-parameter fits use the same gapless stripe-model branch, for which the energy at $(0.25, 0.25)$ vanishes as a model constraint. The close agreement between the two fitted band tops shows that the reduced magnetic energy scale is robust against the choice of fitting parameterization. We therefore focus on the band-top energy and effective exchange scale rather than on the individual microscopic couplings. Taken together, the common-scale and free-parameter fits support the semi-quantitative conclusion that the effective magnetic exchange scale is reduced in $La_2SmNi_2O_7$. Since the interlayer Ni–Ni distance shows no appreciable change between $La_3Ni_2O_7$ and $La_2SmNi_2O_7$, this reduction points to the Ni–O_{AP}–Ni bond geometry as an important structural factor influencing the magnetic exchange scale in bilayer nickelates.

The linewidths provide an additional measure of the coherence of the spin excitations. The resolution-convolved DHO fits yield intrinsic damping parameters $\gamma_q \approx 6.3$–8.8 meV for $La_2SmNi_2O_7$ [green diamonds in Fig. 3]. These values are substantially smaller than the corresponding mode energies, $E_{0,q} \approx 51.4$–61.5 meV, with $\gamma_q/E_{0,q} \approx 0.10$–$0.15$, placing the excitations in the weakly damped regime. The small intrinsic damping supports a spin-wave description of the well-defined magnetic modes, rather than an overdamped continuum response. Together with their clear dispersion, the weak damping indicates that the spin dynamics retain a coherent, local-moment-like component in the presence of itinerant electronic degrees of freedom. This coexistence of itinerant electronic degrees of freedom and well-defined magnetic modes highlights the importance of electronic correlations in bilayer nickelates and provides a reference for tracking their evolution toward the pressure-induced metallic and superconducting states.

In summary, Ni-L_3-edge RIXS measurements on $La_2SmNi_2O_7$ reveal distinct responses of electronic and magnetic excitations to Sm-induced structural distortion. Despite its enhanced in-plane lattice distortion and reduced interlayer Ni–O_{AP}–Ni bond angle compared with $La_3Ni_2O_7$, the electronic features associated with local crystal-field and charge-transfer processes occur at similar energies in the two compounds, including the low-energy 0.3–0.4 eV mode, the ~ 1 eV dd excitation, and the 1.5 eV feature. This shows that Sm substitution does not substantially alter the local NiO_6 electronic energy scales of the corner-shared bilayer. By contrast, the spin-excitation band top is reduced in $La_2SmNi_2O_7$. Analysis using a bilayer J_c-J_1-J_2 Heisenberg model shows that the effective magnetic exchange scale is reduced by about 10%, in correlation with the decrease of the reported interlayer Ni–O_{AP}–Ni bond angle from approximately 168° to 164.2°. The well-defined magnetic modes and their small intrinsic damping further indicate that the low-energy spin dynamics retain a coherent, local-moment-like component in this distorted bilayer nickelate. These results reveal a dichotomy in the response to Sm substitution, with largely preserved local electronic excitation energies but a reduced magnetic exchange scale. They point to the Ni–O_{AP}–Ni geometry as an important structural factor influencing magnetism in Ruddlesden–Popper nickelates and provide spectroscopic constraints for microscopic models of high-T_c superconductivity in this family.

Acknowledgments

This work was supported by the Scientific Research Innovation Capability Support Project for Young Faculty (ZYGXQNJSKYCXNLZCXM-M2), the Natural Science Foundation of Shandong Province, China (Grant No. ZR2026ZD32), the National Key Projects for Research and Development of China with Grant No. 2021YFA1400400, and the National Natural Science Foundation of China (Grants Nos. 12574142, 12374457 and 12074219). The work at PSI was supported by the Swiss National Science Foundation through project Nos. 207904 and 10008343. The RIXS experiments at the BL02U beamline of the NanoTerasu synchrotron facility were performed with the approval of the Japan Synchrotron Radiation Research Institute (JASRI) (Proposal No. 2026A9069). The precise temperature control system used during the experiments at BL02U was developed under Proposal Nos. 2025A9505, 2025B9501, and 2026A9505. We thank Mr. Rei Tanabe of JASRI for technical support during the measurements.

Author contributions

X.L., T.S., and J.Z. conceived this project. J.Y. and J.Z. prepared the samples. X.H., Z.Z., R.L., Y.L., A.C., H.Z., T.S. and X.L. performed the RIXS experiments with the help from H.S., D.F. and J.M.. X.H, and X.L. analysed the data. X.L., Z.Y. and D.-X.Y. conducted the theoretical analysis. X.L. and X.H. wrote the manuscript with inputs from T.S., J.Z.. All authors made comments.

* These authors contributed equally to this work.
† junjie@sdu.edu.cn
‡ thorsten.schmitt@psi.ch
§ luxy@bnu.edu.cn

[1] H. Sun, M. Huo, X. Hu, J. Li, Z. Liu, Y. Han, L. Tang, Z. Mao, P. Yang, B. Wang, J. Cheng, D.-X. Yao, G.-M. Zhang, and M. Wang, Signatures of superconductivity near 80 K in a nick-

elate under high pressure, Nature **621**, 493 (2023).
[2] Y. Zhang, D. Su, Y. Huang, Z. Shan, H. Sun, M. Huo, K. Ye, J. Zhang, Z. Yang, Y. Xu, Y. Su, R. Li, M. Smidman, M. Wang, L. Jiao, and H. Yuan, High-temperature superconductivity with zero resistance and strange-metal behaviour in $La_3Ni_2O_{7-\delta}$, Nat. Phys. **20**, 1269–1273 (2024).
[3] G. Wang, N. N. Wang, X. L. Shen, J. Hou, L. Ma, L. F. Shi, Z. A. Ren, Y. D. Gu, H. M. Ma, P. T. Yang, Z. Y. Liu, H. Z. Guo, J. P. Sun, G. M. Zhang, S. Calder, J.-Q. Yan, B. S. Wang, Y. Uwatoko, and J.-G. Cheng, Pressure-induced superconductivity in polycrystalline $La_3Ni_2O_{7-\delta}$, Phys. Rev. X **14**, 011040 (2024).
[4] M. Shi, D. Peng, Y. Li, S. Yang, Z. Xing, Y. Wang, K. Fan, H. Li, R. Wu, B. Ge, Z. Zeng, Q. Zeng, J. Ying, T. Wu, and X. Chen, Spin density wave rather than tetragonal structure is prerequisite for superconductivity in $La_3Ni_2O_{7-\delta}$, Nature Communications **16**, 9141 (2025).
[5] J. Li, D. Peng, P. Ma, H. Zhang, Z. Xing, X. Huang, C. Huang, M. Huo, D. Hu, Z. Dong, X. Chen, T. Xie, H. Dong, H. Sun, Q. Zeng, H.-k. Mao, and M. Wang, Identification of the superconductivity in bilayer nickelate $La_3Ni_2O_7$ under high pressure up to 100 GPa, Natl. Sci. Rev. **12**, nwaf220 (2025).
[6] N. Wang, G. Wang, X. Shen, J. Hou, J. Luo, X. Ma, H. Yang, L. Shi, J. Dou, J. Feng, J. Yang, Y. Shi, Z. Ren, H. Ma, P. Yang, Z. Liu, Y. Liu, H. Zhang, X. Dong, Y. Wang, K. Jiang, J. Hu, S. Nagasaki, K. Kitagawa, S. Calder, J. Yan, J. Sun, B. Wang, R. Zhou, Y. Uwatoko, and J. Cheng, Bulk high-temperature superconductivity in pressurized tetragonal $La_2PrNi_2O_7$, Nature **634**, 579–584 (2024).
[7] F. Li, Z. Xing, D. Peng, J. Dou, N. Guo, L. Ma, Y. Zhang, L. Wang, J. Luo, J. Yang, J. Zhang, T. Chang, Y.-S. Chen, W. Cai, J. Cheng, Y. Wang, Y. Liu, T. Luo, N. Hirao, T. Matsuoka, H. Kadobayashi, Z. Zeng, Q. Zheng, R. Zhou, Q. Zeng, X. Tao, and J. Zhang, Bulk superconductivity up to 96 K in pressurized nickelate single crystals, Nature **649**, 871–878 (2025).
[8] Q. Zhong, J. Chen, Z. Qiu, J. Li, X. Huang, P. Ma, M. Huo, H. Dong, S. Deng, L. He, Y. Han, H. Sun, and M. Wang, Evolution of superconductivity evidence in pressurized $La_{3-x}Sm_xNi_2O_7$, Phys. Rev. B **113**, 174512 (2026).
[9] Z. Qiu, J. Chen, D. V. Semenok, Q. Zhong, D. Zhou, J. Li, P. Ma, X. Huang, M. Huo, T. Xie, X. Chen, H.-k. Mao, V. V. Struzhkin, H. Sun, and M. Wang, High-temperature superconductivity at 100k in $la_{3-x}nd_xni_2o_7$, Nature Communications (2026).
[10] Z. Pan, C. Lu, F. Yang, and C. Wu, Effect of rare-earth element substitution in superconducting $R_3Ni_2O_7$ under pressure, Chinese Phys. Lett. **41**, 087401 (2024).
[11] E. K. Ko, Y. Yu, Y. Liu, L. Bhatt, J. Li, V. Thampy, C.-T. Kuo, B. Y. Wang, Y. Lee, K. Lee, J.-S. Lee, B. H. Goodge, D. A. Muller, and H. Y. Hwang, Signatures of ambient pressure superconductivity in thin film $La_3Ni_2O_7$, Nature **638**, 935–940 (2025).
[12] G. Zhou, W. Lv, H. Wang, Z. Nie, Y. Chen, Y. Li, H. Huang, W.-Q. Chen, Y.-J. Sun, Q.-K. Xue, and Z. Chen, Ambient-pressure superconductivity onset above 40 K in $(La,Pr)_3Ni_2O_7$ films, Nature **640**, 641–646 (2025).
[13] Y. Liu, E. K. Ko, Y. Tarn, L. Bhatt, J. Li, V. Thampy, B. H. Goodge, D. A. Muller, S. Raghu, Y. Yu, and H. Y. Hwang, Superconductivity and normal-state transport in compressively strained $La_2PrNi_2O_7$ thin films, Nat. Mater. **24**, 1221–1227 (2025).
[14] B. Hao, M. Wang, W. Sun, Y. Yang, Z. Mao, S. Yan, H. Sun, H. Zhang, L. Han, Z. Gu, J. Zhou, D. Ji, and Y. Nie, Superconductivity in Sr-doped $La_3Ni_2O_7$ thin films, Nat. Mater. **24**, 1756–1762 (2025).
[15] G. Zhou, H. Wang, H. Huang, Y. Chen, F. Peng, W. Lv, Z. Nie, W. Wang, J.-F. Jia, Q.-K. Xue, and Z. Chen, Superconductivity onset above 60 K in ambient-pressure nickelate films, National Science Review **13**, nwag151 (2026).
[16] X. Chen, J. Choi, Z. Jiang, J. Mei, K. Jiang, J. Li, S. Agrestini, M. Garcia-Fernandez, H. Sun, X. Huang, D. Shen, M. Wang, J. Hu, Y. Lu, K.-J. Zhou, and D. Feng, Electronic and magnetic excitations in $La_3Ni_2O_7$, Nat. Commun. **15**, 9597 (2024).
[17] Z. Luo, X. Hu, M. Wang, W. Wú, and D.-X. Yao, Bilayer two-orbital model of $La_3Ni_2O_7$ under pressure, Phys. Rev. Lett. **131**, 126001 (2023).
[18] P. Li, G. Zhou, W. Lv, Y. Li, C. Yue, H. Huang, L. Xu, J. Shen, M. Yu, W. Song, Z. Nie, Y. Chen, H. Wang, W. Chen, Y. Huang, Z.-Y. Chen, Q. Tian, J. Lin, J. He, Y.-J. Sun, Z. Chen, and Q.-K. Xue, Angle-resolved photoemission spectroscopy of superconducting $(La,Pr)_3Ni_2O_7/SrLaAlO_4$ heterostructures, Natl. Sci. Rev. **12**, nwaf205 (2025).
[19] B. Y. Wang, S. N. Abadi, Y. Liu, Y. Zhang, Y. Zhong, Y. Yu, B. H. Goodge, X. Zhang, Y.-M. Wu, R. Wang, J. Li, Y. Tarn, E. K. Ko, V. Thampy, C. Lin, M. Hashimoto, D. Lu, Y. S. Lee, T. P. Devereaux, C. Jia, H. Y. Hwang, and Z.-X. Shen, Electronic structure of compressively strained bilayer nickelate thin film, Phys. Rev. X **16**, 031008 (2026).
[20] Y. Wang, K. Jiang, J. Ying, T. Wu, J. Cheng, J. Hu, and X. Chen, Recent progress in nickelate superconductors, Natl. Sci. Rev. **12**, nwaf373 (2025).
[21] Z. Liu, M. Huo, J. Li, and et al., Electronic correlations and partial gap in the bilayer nickelate $La_3Ni_2O_7$, Nat. Commun. **15**, 7570 (2024).
[22] J. Yang, H. Sun, X. Hu, Y. Xie, T. Miao, H. Luo, H. Chen, B. Liang, W. Zhu, G. Qu, C.-Q. Chen, M. Huo, Y. Huang, S. Zhang, F. Zhang, F. Yang, Z. Wang, Q. Peng, H. Mao, G. Liu, Z. Xu, T. Qian, D.-X. Yao, M. Wang, L. Zhao, and X. J. Zhou, Orbital-dependent electron correlation in double-layer nickelate $La_3Ni_2O_7$, Nat. Commun. **15**, 4373 (2024).
[23] Y. Zhang, L.-F. Lin, A. Moreo, and E. Dagotto, Electronic structure, dimer physics, orbital-selective behavior, and magnetic tendencies in the bilayer nickelate superconductor $La_3Ni_2O_7$ under pressure, Phys. Rev. B **108**, L180510 (2023).
[24] V. Christiansson, F. Petocchi, and P. Werner, Correlated electronic structure of $La_3Ni_2O_7$ under pressure, Phys. Rev. Lett. **131**, 206501 (2023).
[25] F. Lechermann, J. Gondolf, S. Bötzel, and I. M. Eremin, Electronic correlations and superconducting instability in $La_3Ni_2O_7$ under high pressure, Phys. Rev. B **108**, L201121 (2023).
[26] D. A. Shilenko and I. V. Leonov, Correlated electronic structure, orbital-selective behavior, and magnetic correlations in double-layer $La_3Ni_2O_7$ under pressure, Phys. Rev. B **108**, 125105 (2023).
[27] Y. Cao and Y.-f. Yang, Flat bands promoted by Hund's rule coupling in the candidate double-layer high-temperature superconductor $La_3Ni_2O_7$ under high pressure, Phys. Rev. B **109**, L081105 (2024).
[28] Q. Qin and Y.-F. Yang, High-T_c superconductivity by mobilizing local spin singlets and possible route to higher T_c in pressurized $La_3Ni_2O_7$, Phys. Rev. B **108**, L140504 (2023).
[29] C. Lu, Z. Pan, F. Yang, and C. Wu, Interlayer-coupling-driven high-temperature superconductivity in $La_3Ni_2O_7$ under pressure, Phys. Rev. Lett. **132**, 146002 (2024).
[30] Y.-f. Yang, G.-M. Zhang, and F.-C. Zhang, Interlayer valence bonds and two-component theory for high-T_c superconductivity of $La_3Ni_2O_7$ under pressure, Phys. Rev. B **108**, L201108

(2023).
[31] Y. Shen, M. Qin, and G.-M. Zhang, Effective bi-layer model hamiltonian and density-matrix renormalization group study for the high-T_c superconductivity in $La_3Ni_2O_7$ under high pressure, Chinese Phys. Lett. **40**, 127401 (2023).
[32] L. Chen, E. Zhang, Y. Hao, Y. Zhu, B. Cui, D. L. Abernathy, T. J. Williams, Y. Ikeda, H. Zhang, F. Liu, W. Wang, Q. Wang, and J. Zhao, Nature of magnetism in bilayer nickelate $La_3Ni_2O_7$ single crystals (2026), arXiv:2605.03448 [cond-mat.str-el].
[33] I. Plokhikh, T. J. Hicken, L. Keller, V. Pomjakushin, S. H. Moody, P. Foury-Leylekian, J. J. Krieger, H. Luetkens, Z. Guguchia, R. Khasanov, and D. J. Gawryluk, Unraveling spin density wave order in layered nickelates $La_3Ni_2O_7$ and $La_2PrNi_2O_7$ via neutron diffraction (2025), arXiv:2503.05287.
[34] N. K. Gupta, R. Gong, Y. Wu, M. Kang, C. T. Parzyck, B. Z. Gregory, N. Costa, R. Sutarto, S. Sarker, A. Singer, D. G. Schlom, K. M. Shen, and D. G. Hawthorn, Anisotropic spin stripe domains in bilayer $La_3Ni_2O_7$, Nat. Commun. **16**, 6560 (2025).
[35] X. Ren, R. Sutarto, X. Wu, J. Zhang, H. Huang, T. Xiang, J. Hu, R. Comin, X. Zhou, and Z. Zhu, Resolving the electronic ground state of $La_3Ni_2O_{7-\delta}$ films, Commun. Phys. **8**, 52 (2025).
[36] X.-S. Ni, Y. Ji, L. He, T. Xie, D.-X. Yao, M. Wang, and K. Cao, Spin density wave in the bilayered nickelate $La_3Ni_2O_{7-\delta}$ at ambient pressure, npj Quantum Mater. **10**, 17 (2025).
[37] J. Huang, S. Ramakrishnan, P. Rodière, P. Toulemonde, Z. Rahmany, V. Balédent, B. Vignolle, S. Marik, P. Fertey, and P. Foury-Leylekian, Pressure-driven structural transitions without a displacive charge-density wave in $La_2SmNi_2O_7$ (2026), arXiv:2607.03363 [cond-mat.str-el].
[38] H. Zhou, X. Ye, G. Wang, D. Adroja, D. Tam, M. M. Koza, Z. Lu, J. Cheng, D.-X. Yao, and H. Luo, Spin fluctuations in the rare-earth doped bilayer nickelates, Science China Physics, Mechanics & Astronomy **69**, 277411 (2026).
[39] W. Wú, Z. Luo, D.-X. Yao, and M. Wang, Superexchange and charge transfer in the nickelate superconductor $La_3Ni_2O_7$ under pressure, Sci. China Phys. Mech. Astron. **67**, 117402 (2024).
[40] H. Zhong, B. Hao, Z. Zhang, A. Chen, Y. Wei, R. Liu, X. Huang, C. Li, W. Zhang, C. Liu, X.-S. Ni, M. dos Reis Cantarino, K. Kummer, N. Brookes, K. Cao, Y. Nie, T. Schmitt, and X. Lu, Spin correlations in $La_3Ni_2O_7$ thin films (2026), arXiv:2502.03178 [cond-mat.supr-con].
[41] L. Bhatt, E. Abarca Morales, A. Y. Jiang, E. K. Ko, Y.-F. Zhao, N. Schnitzer, G. A. Pan, D. Ferenc Segedin, Y. Liu, Y. Yu, C. M. Brooks, A. S. Botana, H. Y. Hwang, J. A. Mundy, D. A. Muller, and B. H. Goodge, Structural modifications in strain-engineered bilayer nickelate thin films, Nature **653**, 76–82 (2026).
[42] Y. Zhong, W. Wú, and D.-X. Yao, Superexchanges and charge transfer in $La_3Ni_2O_7$ thin films, Chinese Physics Letters **43**, 030713 (2026).
[43] X.-W. Yi, W. Li, J.-Y. You, B. Gu, and G. Su, Unifying strain- and pressure-driven superconductivity in $La_3Ni_2O_7$: Suppressed charge and spin density waves and enhanced interlayer coupling, Phys. Rev. B **112**, L140504 (2025).
[44] D.-C. Lu, M. Li, Z.-Y. Zeng, W. Hou, J. Wang, F. Yang, and Y.-Z. You, Superconductivity from doping symmetric mass generation insulators: Application to $La_3Ni_2O_7$ under pressure (2023), arXiv:2308.11195.
[45] J.-X. Zhang, H.-K. Zhang, Y.-Z. You, and Z.-Y. Weng, Strong pairing originated from an emergent $\mathbb{Z}_2$ berry phase in $La_3Ni_2O_7$, Phys. Rev. Lett. **133**, 126501 (2024).

Supplementary Files

This is a list of supplementary files associated with this preprint. Click to download.

- RIXSLa2SmNi2O7260927SI.pdf